Synthesis, characterization and catalytic activities of mesoporous AlMSU-X with wormhole-like framework structure

Shang-Ru Zhai, Wei Wei, Dong Wu, and Yu-Han Sun*

State Key Laboratory of Coal Conversion, Institute of Coal Chemistry, Chinese Academy of Sciences, Taiyuan 030001, China

Received 5 May 2003; accepted 23 June 2003

Mesoporous AlMSU-X molecular sieves with high acidity have been prepared from preformed beta nanoclusters under strong acidic conditions in the presence of nonionic TX-100 as structure directors. These materials were characterized by XRD, HRTEM, N_2-adsorption, ^{27}Al MAS NMR, NH_3-TPD, IR-pyridine adsorption and catalytic cracking of cumene and 1,3,5-triisopropylbenzene. The experimental results showed that Al heteroatoms had been successfully incorporated into the framework structure of mesoporous MSU-X, and so-produced catalysts exhibited superior catalytic properties.

KEY WORDS: mesoporous; AlMSU-X; high acidity; cracking; cumene; 1,3,5-triisopropylbenzene.

1. Introduction

Recently, many efforts have been devoted to improving the activity of mesoporous aluminosilicates in acid-catalyzed reactions [1–11]. One of such approaches consists in mimicking the physicochemical conditions prevalent in the synthesis gels from which zeolite materials are obtained, and then promoting the surfactant-assisted assembly of the zeolite precursors present in the gel. In this way, mesostructured materials analogous to MCM-41, SBA-15, and MCF characterized by enhanced acidity have been prepared from MFI, BEA, and FAU seeds [5–11]. However, these materials are all made of unidimensionally packed cylindrical channels [5–11], from the catalysis point of view, and appear to be inferior to mesoporous aluminosilicates with a 3D porosity such as MCM-48 (cubic symmetry) and MSU-X (3D wormhole porosity). Though an MCM-48-like mesoporous material with high acidity has been obtained using BEA seeds as inorganic species [12], the synthesis carried out under high pH (~11.2) condition is unfavorable due to under which zeolite seeds can easily grow into large crystals. If the synthesis conditions is not controlled very well, a mixture of zeolite and MCM-48 would be obtained.

In order to avoid the aforementioned disadvantages, the present work is focused on the synthesis of 3D wormhole AlMSU-X materials by a two-step synthesis procedure. In the first step, precursors containing beta nanoclusters were prepared according to the reported procedure [6], and then the preformed zeolite seeds were assembled into mesostructure in the presence of TX-100 in acid media (pH < 0). The advantage of this route is that the zeolite seeds prepared in the first step cannot grow continuously into large crystals under the extremely acidic condition in the second step and in turn, the products will be pure mesophase without zeolite as by-products; as a result, the aluminum in the framework is mostly at zeolite-like sites, which lead to the high catalytic activity.

* To whom correspondence should be addressed.
E-mail: yhsun@sxicc.ac.cn

2. Experimental

2.1. Preparation

The synthesis procedure involves the preparation of a solution precursor of beta with the following molar composition Al_2O_3: 20.0 TEAOH: 2.11 Na_2O: 44.44 SiO_2: 613 H_2O. In a typical synthesis, 2.40 g of fumed silica was slowly dissolved in a solution containing 10.58 g of a 25 wt% TEAOH aqueous solution, 0.158 g $NaAlO_2$, 0.08 g NaOH and 2.00 g distilled water and after being stirred for 4 h at room temperature, then the opalescent mixture obtained was poured into Teflon-lined autoclave and heated at 140 °C for 6 h, yielding clear aluminosilicate precursors.

The above clear solution was mixed at room temperature with 150.99 g of a 4.63 wt% TX-100 aqueous solution followed by addition of 24.2, 30.2, and 36.3 mL of HCl (11.9 M), respectively, and after the reaction mixture was stirred for 6 h. The precipitate was recovered by filtration, washed by water and then loaded into an autoclave for additional reaction at 110 °C for 48 h. Finally, the solid was filtered, air dried and calcined at 550 °C for 6 h to remove the template. The final molar ratios of the gel were SiO_2: 0.0225 Al_2O_3: 0.45 TEAOH: 0.047 Na_2O: 0.27 TX-100: x HCl: 213.8 H_2O ($x = 7.2$, 9.0, and 10.8). Corresponding to $x = 7.2$, 9.8, and 10.8, three samples denoted as **a**, **b**, and

1011-372X/03/0900–0261/0 © 2003 Plenum Publishing Corporation

c were represented and characterized by a series of measurements. The proton form of the sample was prepared from ion exchange of NH_4NO_3 (1M), followed by calcination at 550 °C for 3 h.

2.2. Characterization

2.2.1. Structure

XRD measurements were performed on a D/max-rA instrument with Cu Kα radiation, scanning speed at 0.02° with a count time of 0.5 s at each time, and scanning regions at 1–5° and 5–40°. HRTEM was performed on a Philips CM-200 FEG instrument operated at 200 kV. The BET surface area and pore-size distribution of the samples were measured with a Micromeritics Tristar 3000 system using nitrogen as the analysis gas at 77 K. The pore-size distribution curves were obtained from the desorption branches of the isotherms using the conventional BJH model. Solid-state ^{27}Al MAS NMR was performed on a Bruker MSL-300WB spectrometer, and chemical shifts were referenced to $Al(H_2O)_6^{3+}$.

2.2.2. Acidity

NH_3-TPD was performed on 200 mg of the catalyst with nitrogen (40 mL/min) as the carrier gas and a thermoconductor as the detector. NH_3-TPD curves were obtained in the range 120–600 °C with a heating rate of 10 °C/ min. IR-pyridine adsorption was obtained on a FTS-25PC spectrometer. The self-supporting wafers about 5 mg/cm^2 were evacuated *in situ* in an IR cell at 350 °C for 4 h and cooled to room temperature. Then pyridine was exposed to the disks at room temperature. After the adsorption at room temperature for 0.5 h and evacuation at 150, 250, and 350 °C for different time, the spectra were recorded.

2.2.3. Catalytic test

Catalytic cracking of cumene and 1,3,5-triisopropylbenzene were carried out at 300 °C by pulse method to evaluate the catalytic performance of the samples. In each run, 60 mg of catalyst was used, the pulse injection of the reactant was 0.2 μL, and nitrogen was used as carrier gas at a flowing rate of 50 mL/min. The catalytic products were analyzed using GC-9A (Shimazu Co.) equipped with a Chrom-Workstation Data Set.

3. Results and discussion

3.1. Textural properties

The powder XRD patterns of calcined AlMSU-X materials show a broad peak arising from the average pore–pore separation in the disordered wormhole framework (see figure 1). These patterns are similar to those of MSU-X pure silica assembled from the same surfactant, but only with TEOS as the silica precursor [13,14]. Evidence for disordered, wormhole-like framework pore structure of the AlMSU-X materials is provided by a typical transmission electron micrograph (TEM) image (see figure 2). As can be seen from the micrograph for the sample **b**, the particle contains a large number of channels similar to that in pure MSU-X silica [13,14].

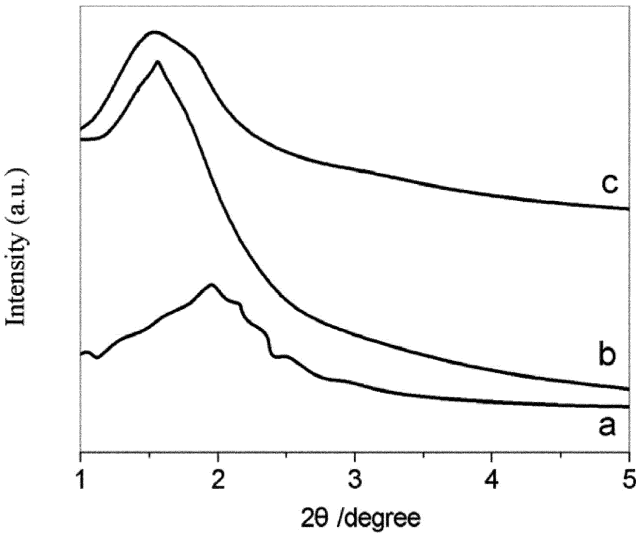

Figure 1. The XRD patterns of calcined samples.

No distinguishable reflection of bulky zeolite crystals in the wide-angle region in XRD pattern suggests that the products are pure mesophase (not shown). This implies that the nanoclusters prepared in the first step cannot grow into crystals large enough to be detected by XRD because of the extremely acidic condition in the second assembly procedure [9–11].

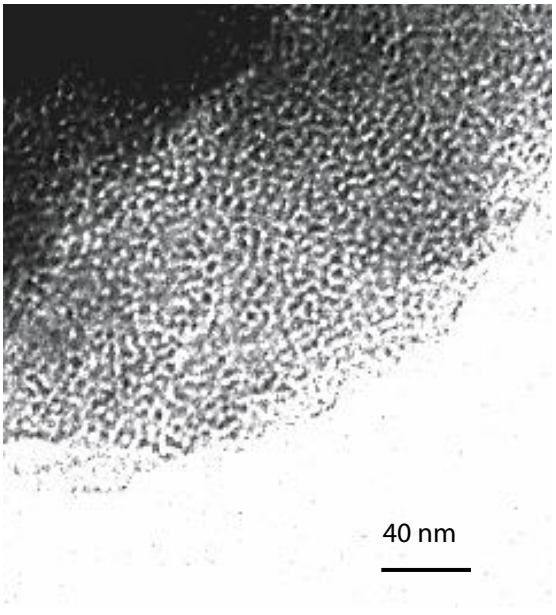

Figure 2. Representative HRTEM image of wormhole pore structure (sample **b**).

The N_2 adsorption–desorption isotherms of calcined AlMSU-X samples are typical of well-defined structural porous framework (see figure 3(a)). One type I and two type IV adsorption isotherms with sharp uptake of N_2 in the range 0.30~0.45 P/P_0 are presented, corresponding to capillary condensation within framework pores with BJH diameters of 22.9, 30.2, and 30.2 Å for sample **a**, **b**, and **c**, respectively (see figure 3(b)). The lack of any additional nitrogen adsorption for the higher relative pressure values means that there is no textural porosity.

Table 1 summarizes the physicochemical properties obtained from XRD and N_2 adsorption. Notably, the pore-wall thickness, as obtained from the difference between the pore–pore correlation distance and pore size, increases with increasing acid concentration in the second step. Such a change is related to the extent of protonation of the PEO block, being a characteristic feature of $N^0(N^+)X^-I^+$ assembly [15]. Under the present synthesis condition, we postulate that the nanoclusters are likely to be completely charged (I^+) by H^+, the surfactant monomers, however, may be just partly protonated because of the pH-insensitive feature of PEO block. Thus, more amount of acid is introduced, more PEO block is protonated and more I^+ can match with the Cl^- interacting with positively charged PEO. As a result, thicker wall and larger pore-size AlMSU-X samples are obtained.

Table 1
Physicochemical properties of the samples

Sample	d_{100} (Å)	Surface area (m^2/g)	Pore size (Å)	Pore volume (cm^3/g)	Wall thickness[a] (Å)
a	45.1	800	22.9	0.44	29.2
b	52.5	747	30.2	0.64	30.4
c	53.6	724	30.2	0.61	31.7

[a]The wall thickness was calculated by subtracting the BJH pore size from the correlation distance.

3.2. *^{27}Al MAS NMR measurement*

^{27}Al MAS NMR is the most revealing method for examining the coordination state of aluminum. The ^{27}Al MAS NMR spectra of samples **a** and **b** exhibit two distinct signals at 58 and 0 ppm (see figure 4). The line at 58 ppm can be assigned to the aluminum in a tetrahedral environment (AlO_4), in which aluminum is covalently bound to four Si atoms via oxygen bridges, whereas the chemical shift at 0 ppm can be attributed to octahedral aluminum (AlO_6) [16,17]. The results clearly show that, for samples **a** and **b**, a large amount of Al is incorporated in the framework, though some nonframework Al is still present. For sample **c**, however, more than 50% of the Al is 6-coordinated and the intensity of the peak corresponding to tetrahedral aluminum decreases a lot; in addition, there is a weak peak at 27 ppm, which can be assigned to 5-coordinated aluminum or alternatively, aluminum in highly distorted tetrahedral sites in dealuminated beta zeolite. It is probably due to this that the acid concentration in the second step is high enough to dealuminate most of Al atoms already fixed in the framework of zeolite seeds. Of

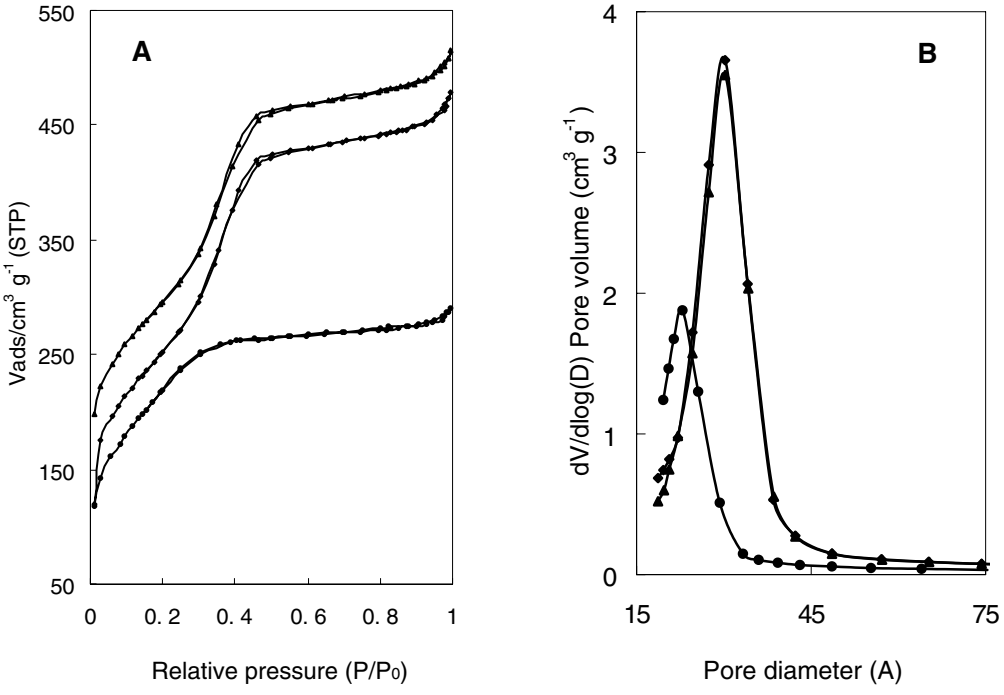

Figure 3. N_2 adsorption/desorption isotherms (A) and pore-size distribution curves (B) of (●) **a**, (◆) **b**, and (▲) **c**.

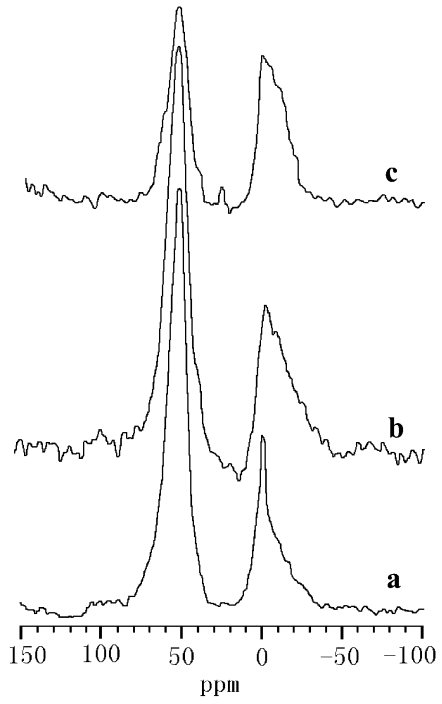

Figure 4. The ^{27}Al MAS NMR spectra of protonated samples.

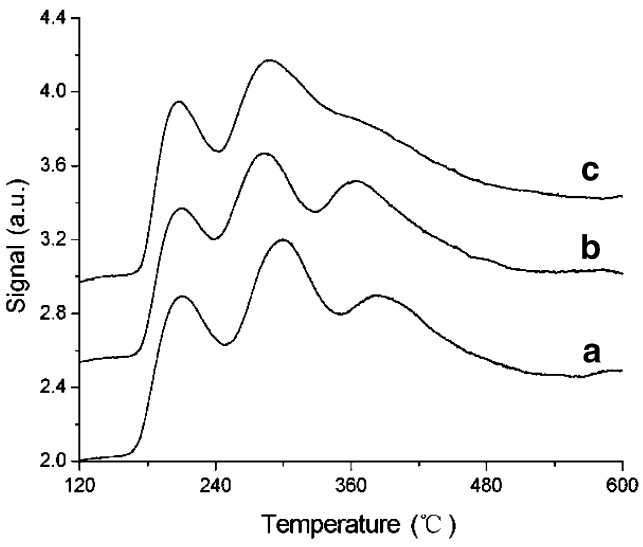

Figure 5. The NH_3-TPD profiles of protonated samples.

interest is the chemical shift of 4-coordinated aluminum in these AlMSU-X catalysts that occurs at 58 ppm (similar to that in zeolite beta, ca. 60 ppm) rather than 51 ppm previously reported for all AlMSU-X obtained by various methods [18], suggesting that the presence of Si–O–Al environments is different from those commonly present in amorphous AlMSU-X [18], which resemble those existing in zeolite beta [9].

3.3. Acidity measurement

The NH_3-TPD profiles of the three samples are compared in figure 5. Obviously, three desorption peaks caused by weak, medium, and strong acid sites, respectively, can be observed for both **a** and **b**. Although sample **c** does not show an intense peak from strong acid sites like **a** and **b**, a prominent shoulder is observed at about 366 °C. These results suggest that the samples contain three different acid sites. Moreover, the acid strength decreases in order: **a** > **b** > **c**. This is well consistent with the aforementioned ^{27}Al MAS NMR analysis that more Al species dealuminate from the framework of the zeolite seeds with higher acid concentration used in the second procedure.

The IR spectra of pyridine adsorbed on protonated samples in the region 1600–1400 cm^{-1} after evacuation at different temperatures exhibited bands because of strong Lewis-bound pyridine at 1452 cm^{-1}, pyridine bound to Brönsted acid sites at 1545 cm^{-1} and a band at 1491 cm^{-1} that can be assigned to pyridine associated with both Brönsted and Lewis sites [3,4,16,19] (see figure 6). Noticeably, the 1545 cm^{-1} peaks associated with Brönsted acid sites still remain resolved on all samples even after desorption at 350 °C for 5 min, indicating that the strength of Brönsted acid sites on these samples is strong, which is well consistent with the NH_3-TPD observation. The order of the acid site density is **a** > **b** > **c**. This is closely related to the amount of aluminum incorporated into the mesostructures in the second assembly step (see ^{27}Al MAS NMR in figure 4).

3.4. Catalytic activity

3.4.1. Catalytic cracking of cumene

The cracking of cumene is chosen as a model reaction to test the activities of the samples. Generally, the catalytic activities decrease with pulse number. The results in figure 7 show the dependence of cumene conversion of fresh sample **a** on the pulse number at 300 °C. At the first pulse number, the catalyst shows high activity, arriving at 48.1%. With increasing the pulse number, however, the catalytic activity over it decreases remarkably. When the pulse number is 30, only 36.3% of the conversion is observed. However, the activity of it could be recovered completely after being treated in dry air at 550 °C for 2 h. It seems that the deactivation is mainly caused by coke deposited on the catalyst surface.

Table 2 presents catalytic activities of various samples in cumene cracking. Obviously, sample **a** shows the highest activity in cumene cracking for the three samples. For instance, sample **a** gives conversion of 36.3%, which is higher than 32.6% of **b** and 18.4% of **c**. This result may be assigned to higher acidity of sample **a** than that of **b** and **c**.

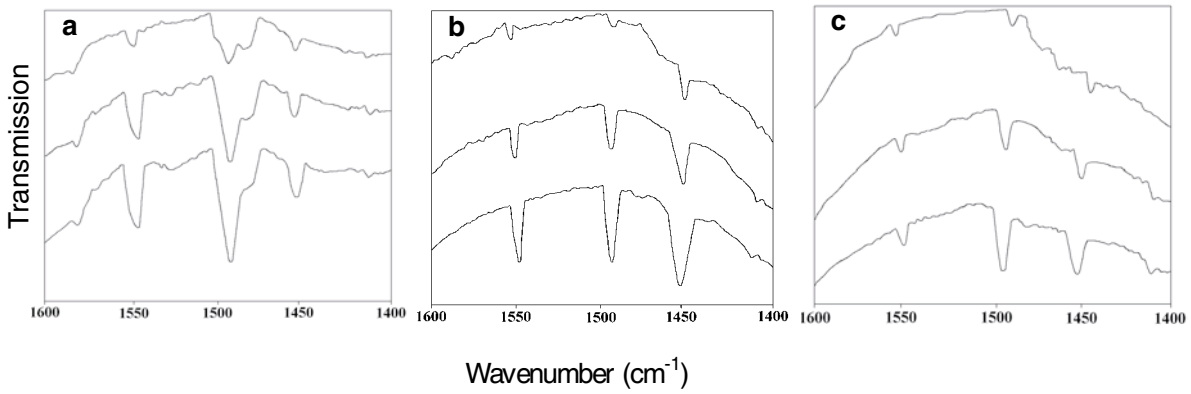

Figure 6. IR spectra of pyridine adsorbed on the samples, and then desorption at different temperature ((bottom): 150 °C/30 min; (middle): 250 °C/20 min; (top): 350 °C/5 min).

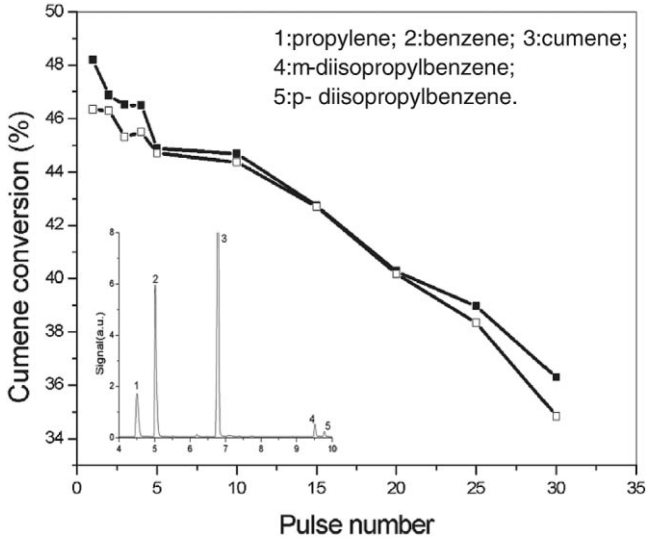

Figure 7. The dependence of catalytic activity on the pulse number in cumene cracking at 300 °C over fresh (■) and regenerated (□) sample **a**. (Insert, products distribution of cumene cracking over sample **a**. Regeneration conditions: heating in air at 550 °C for 2 h.)

Additionally, we observe that there are diisopropylbenzene by-products over both samples **a** and **b**, which may result from catalytic alkylation of isopropylbenzene with propylene formed by cracking of isopropylbenzene (see figure 7, insert: representative products distribution of sample **a**), and this phenomenon was also reported by other researchers [20]. Moreover, sample **a** shows higher selectivity for the diisopropylbenzene products than **b**, which can be attributed to its stronger ability for the alkylation.

3.4.2. Catalytic cracking of 1,3,5-triisopropylbenzene

It is well known that cumene dealkylation is a typical, strong acid-catalyzed reaction [4,8]. In contrast, the molecular 1,3,5-triisopropylbenzene cracking is a weak-to-medium acid-catalyzed reaction [21]. Figure 8 illustrates the dependence of 1,3,5-triisopropylbenzene conversion on the pulse number over fresh and regenerated sample **a**. This result demonstrates that sample **a** exhibits very high activity in 1,3,5-triisopropylbenzene cracking and it can totally recover its activity after being regenerated in air at 550 °C for 2 h.

Catalytic activities of various samples in 1,3,5-triisopropylbenzene cracking at 300 °C are listed in table 3. Indeed, these aluminosilicates exhibit very high activity in 1,3,5-triisopropylbenzene cracking, which can be attributed to the medium and strong acid sites as well as wormlike pore structures they have. Meanwhile, for 1,3,5-triisopropylbenzene cracking the activities decrease in order: **a** > **b** > **c**. This may result from the different number and strength of the acid sites in them.

Table 2
Catalytic activities of various samples in the cracking of cumene at 300 °C

Sample	Conversion (%)[a]	Selectivity (%)			
		Propylene	Benzene	*m*-Diisopropylbenzene	*p*-Diisopropylbenzene
a	36.3	26.8	63.3	6.8	3.1
b	32.6	27.6	63.9	6.0	2.4
c	18.4	26.2	73.8	–	–

Note: Here, (–) means the product is undetectable.
[a]The conversion was the 30th pulse.

Table 3
Catalytic activities in the cracking of 1,3,5-triisopropylbenzene over samples of **a**, **b**, and **c**

Sample	Conversion (%)[a]	Selectivity (%)				
		Propylene	Benzene	Cumene	*m*-Diisopropylbenzene	*p*-Diisopropylbenzene
a	100.0	40.3	3.7	44.2	8.6	3.1
b	99.8	39.1	2.5	41.6	11.2	5.5
c	97.8	33.3	1.7	32.1	24.1	7.8

[a]The conversion was the second pulse.

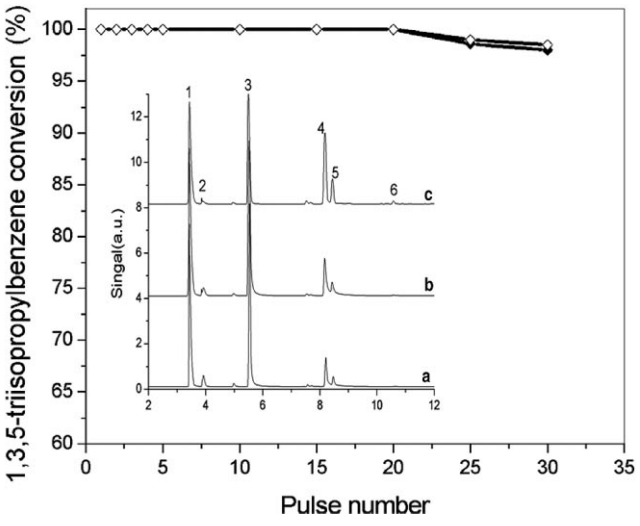

Figure 8. The dependence of catalytic activity on the pulse number in 1,3,5-triisopropylbenzene cracking over fresh (◆) and regenerated (◇) sample **a**. (Insert, 1-5: the same products as in figures 7, 6: 1,3,5-triisopropylbenzene.)

Furthermore, we find that the product distribution is different in 1,3,5-triisopropylbenzene cracking. Although propylene and cumene are the major products for all samples, the selectivity for them varies remarkably relative to different samples. For example, the selectivity for propylene and isopropylbenzene over sample **a** is 40.3% and 44.2%, which is higher than 39.1% and 41.6%, 33.3% and 32.1% for samples **b** and **c**, respectively. At the same time, the selectivity for diisopropylbenzene over these samples increases in order, i.e., **a** < **b** < **c** (see figure 8, insert—the product distribution for the samples). This reasonably results from the difference in acidic properties, acid site density, and cracking mechanisms. These results suggest that the wormhole-like AlMSU-X is an excellent candidate as a catalyst for catalytic cracking of large molecules, particularly of the petroleum residues for which high reaction temperatures are required.

4. Conclusions

Mesoporous AlMSU-X molecular sieves with high acidity have been prepared for the first time under strong acid conditions in the presence of TX-100 as structure directors. Taking ^{27}Al MAS NMR, NH_3-TPD and pyridine-FTIR as well as catalytic performance of these materials into account, the results suggest that the present synthesis gives rise to AlMSU-X-like aluminosilicates of enhanced acidity, their acid strength being nevertheless lower than that of beta. Such materials with three-dimensional wormholes may be suitable for many catalytic processes that do not require strong acid strength, such as mild hydrocracking and cracking of bulky feedstocks.

Acknowledgments

Financial support from the National Natural Science Foundation of China (Grant Number 29625307) and the National Key Basic Research Special Foundation of China (Grant Number 2000048001) is gratefully acknowledged.

References

[1] A. Karlsson, M. Stocker and R. Schmidt, Microporous Mesoporous Mater. 27 (1999) 181.
[2] M.J. Verhoef, P.J. Kooyman, J.C. van der Waal, M.S. Rigutto, J.A. Peters and H. van Beckkum, Chem. Mater. 13 (2001) 683.
[3] D.T. On and S. Kaliaguine, Angew. Chem. Int. Ed. 40 (2001) 3248.
[4] D.T. On and S. Kaliaguine, J. Am. Chem. Soc. 125 (2003) 618.
[5] Y. Liu, W. Zhang and T.J. Pinnavaia, Angew. Chem., Int. Ed. 40 (2001) 1255.
[6] Z. Zhang, Y. Han, L. Zhu, R. Wang, Y. Yu, S. Qiu, D. Zhao and F. Xiao, Angew. Chem., Int. Ed. 40 (2001) 1258.
[7] J. Agundez, I. Diaz, C.M. Alvarez, J.P. Pariente and E. Sastre, J. Chem. Soc., Chem. Commun. (2003) 150.
[8] Y. Liu, W. Zhang and T.J. Pinnavaia, J. Am. Chem. Soc. 122 (2000) 8791.
[9] Y. Han, F. Xiao, S. Wu, Y. Sun, X. Meng, D. Li, S. Lin, F. Deng and X. Ai, J. Phys. Chem., B 105 (2001) 7963.
[10] Y. Liu and T.J. Pinnavaia, Chem. Mater. 14 (2002) 3.
[11] Y. Han, S. Wu, Y. Sun, D. Li and F. Xiao, Chem. Mater. 14 (2002) 1144.
[12] P. Shih, H. Lin and C. Mou, 3rd International Mesostructured Materials Symposium, Korea (2002) p. 10.
[13] S.A. Bagshaw, E. Prouzel and T.J. Pinnavaia, Science 269 (1995) 1242.
[14] S.S. Kim, T.R. Pauly and T.J. Pinnavia, J. Chem. Soc., Chem. Commun. (2000) 835.
[15] D. Zhao, J. Feng, Q. Huo, N. Melosh, G.H. Fredrickson, B.F. Chmelka and G.D. Stucky, Science 279 (1998) 548.

[16] D. Zhao, C. Nie, Y. Zhou, S. Xia, L. Huang and Q. Li, Catal. Today 68 (2001) 11.
[17] Z. Luan, M. Hartmann, D. Zhao, W. Zhou and L. Kevan, Chem. Mater. 11 (1999) 1621.
[18] S. Bagshaw, T. Kemmitt and N. Milestone, Microporous Mesoporous Mater. 22 (1998) 419.
[19] B. Chakraborty, B. Viswanathan, Catal. Today 49 (1999) 253.
[20] L. Zhu, F. Xiao, Z. Zhang, Y. Sun, Y. Han and S. Qiu, Catal. Today 68 (2001) 209.
[21] H. Koch and W. Reschetilowski, Microporous Mesoporous Mater. 25 (1998) 127.